Determination of the beam asymmetry Σ in η- and η'-photoproduction

Jakob Michael Krause

Masterarbeit in Physik
angefertigt im Helmholtz-Institut für Strahlen- und Kernphysik

vorgelegt der
Mathematisch-Naturwissenschaftlichen Fakultät
der
Rheinischen Friedrich-Wilhelms-Universität
Bonn

Sep 2022

I hereby declare that this thesis was formulated by myself and that no sources or tools other than those cited were used.

Bonn, ...
Date Signature

1. Gutachterin: Jun. Prof. Dr. Annika Thiel
2. Gutachter: Prof. Dr. Jochen Dingfelder

Contents

CHAPTER 3

Event selection

The determination of polarization observables needs to be completed for particular reactions (cf. chapter 1), such as the photoproduction of e.g. a single η' meson. However, the recorded events contain data from the decay products of all possible final states in addition to combinatorical background. Thus, event candidates for the desired reaction have to be extracted before they are considered for further analysis. Table 3.1 shows the five most probable decay modes of the η' meson. Three of these result in final states which only contain photons and are thus reliably measurable with the CBELSA/TAPS experiment. Only the $\eta' \to \gamma\gamma$ decay channel was considered for further analysis; the $\omega\gamma$ channel provides negligible statistics and considering the acceptance of detecting six photons in the final state, the expected yield of the $\eta' \to \gamma\gamma$ decays should be roughly equal to the $\eta' \to \pi^0\pi^0\eta \to 6\gamma$ final state [Afz22]. Offering a cleaner, three-particle final state, the $\eta' \to \gamma\gamma$ channel was then favored in the course of this thesis.

Decay mode			Branching ratio
$\pi^+\pi^-\eta$			42.6%
$\rho^0\gamma$	$\to$	$\pi^+\pi^-\gamma$	28.9% (28.9%)
$\pi^0\pi^0\eta$	$\to$	6γ	22.8% (8.8%)
$\omega\gamma$	$\to$	$\pi^+\pi^-\pi^0\gamma/\pi^0\gamma\gamma$	2.52% (2.2%/0.21%)
$\gamma\gamma$			2.3%

Table 3.1: The five most probable decay modes of the η' meson. The most probable further decay with according branching ratio is shown in brackets.[Zyl+20]

The process of *event selection* for the reaction $\gamma p \to p\eta' \to p\gamma\gamma$ is outlined in the following chapter. Note that in this thesis the analysis of data from η-photoproduction starts with this process already completed, which is described in detail in reference [Afz19].

3.1 Preselection and charge cut

Since the polarization degree can only be evaluated reliably up to 1 800 MeV and the production threshold for η' mesons is E_γ = 1 447 MeV [Zyl+20], the beam photon energy range was restricted to 1 400 to 1 800 MeV from the very beginning. The measured events are then generally classified

depending on the number of particle energy deposits (PED). If the complete four-momenta of three final state particles are measured, they are referred to as 3PED events. Low energy protons however may either be only detected in the scintillators of the inner, forward or MiniTAPS detector – giving only directional information (2.5 PED) – or lost entirely (2 PED). Only 2.5PED and 3PED events were analyzed since the additional background contributions from 2PED events exceeded the additional signal contributions. It is worth noting that 3PED events are significantly dominant for $\eta' \to \gamma\gamma$ reactions; the production threshold for η' mesons is so high energetic that the recoil proton will likely be detected. Figure 3.1 shows the distribution of the different event classes for $\eta' \to \gamma\gamma$ production in MONTE CARLO data, with a clear preference towards 3PED events.

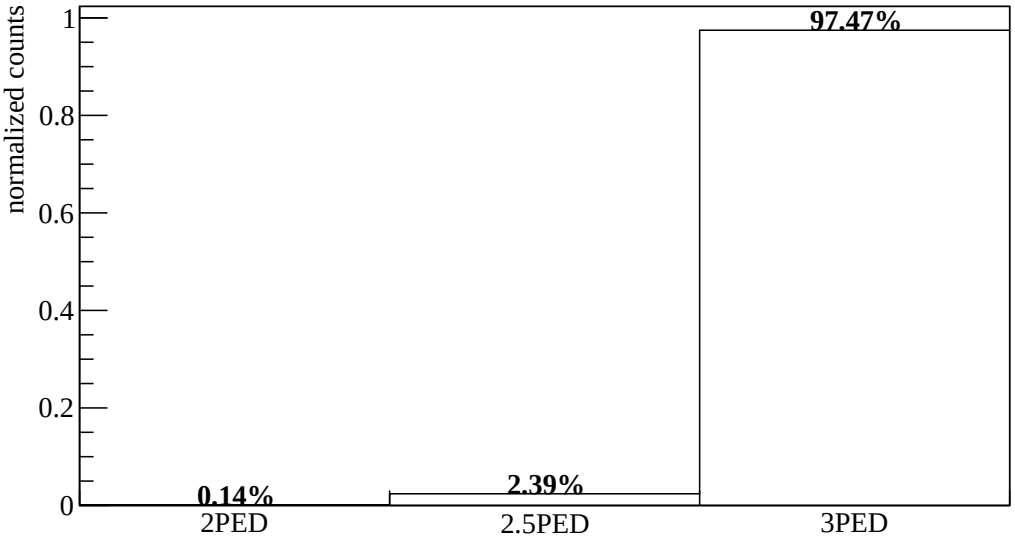

Figure 3.1: Distribution of event classes in $\eta' \to \gamma\gamma$ production

To further improve the signal to background ratio, the charge information of the final state particles was utilized in the next step. In particular, to select $\eta' \to \gamma\gamma$ reactions, one charged and two uncharged particles in the final state were demanded.

3.2 Time of particles

Due to its high count rate the tagging system (see section 2.1.1) will not only record beam photons which produce the detectable final state particles, but also several uncorrelated ones. To select only beam photons which will induce a photoproduction process the time information of the detected particles is used. It is shown in figure 3.2 for all particles involved in 2.5PED and 3PED events of η' photoproduction. In all cases prompt peaks centered around 0 ns (the trigger time) are visible. Since the final state photons move with velocity c their timing information does not underlie fluctuations, as is the case for the final state proton on the contrary. The tagged, uncorrelated beam photons are visible as flat background underneath the prompt peak in the time of the beam photon. Naturally, only coincident events may be referred to as η' candidates for the further analysis and thus only events

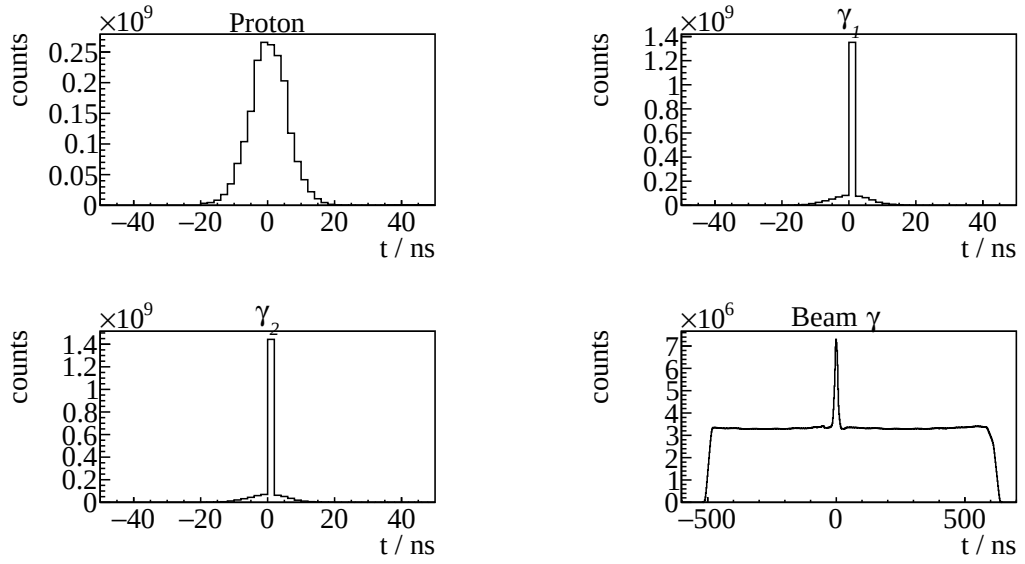

Figure 3.2: Time information of all final state particles and the beam photon for 3PED η' production

with time information of at least one final state particle are kept. Photons need to be detected in the MiniTAPS or forward detector to acquire time information. To determine coincidence it is convenient to define the *reaction time*

$$t_{\text{reaction}} = \begin{cases} t_{\text{beam}} - t_{\text{meson}} & \text{meson time exists} \\ t_{\text{beam}} - t_{\text{recoil}} & \text{meson time does not exist,} \end{cases} \tag{3.1}$$

where the meson time t_{meson} is appointed either the averaged time of both decay photons or the time of a single photon if only one photon has time information. t_{beam} and t_{recoil} are the time of the beam photon and recoil proton, respectively. Figure 3.3 shows the reaction time for 2.5PED and 3PED events; a clear prompt peak centred at 0 is visible, the colored area indicates the chosen range of $t_{\text{reaction}} \in [-8, 5]$ns. However, this cut still contains random time background underneath the prompt peak. This may be accounted for by *sideband substraction*, assuming the background is flat. All events residing in the prompt peak with $t_r \in [-8, 5]$ns will be assigned a weight of $w_p = +1$ while sideband events with $t_r \in [-200, -100]\text{ns} \vee t_r \in [100, 200]$ns will be assigned a weight of $w_s = -\frac{13}{200}$. Any histogram N that is filled in the following will then consist of prompt peak events N_{prompt} and sideband events N_{sideband}

$$N = N_{\text{prompt}} + w_s \cdot N_{\text{sideband}},$$

such that the random time background underneath the prompt peak is substracted. In addition, the time difference between meson and proton and between the two photons is demanded to be within $[-10, 10]$ns. All described cuts to the data, including the sideband substraction are referred to as the *time cut* in the following.

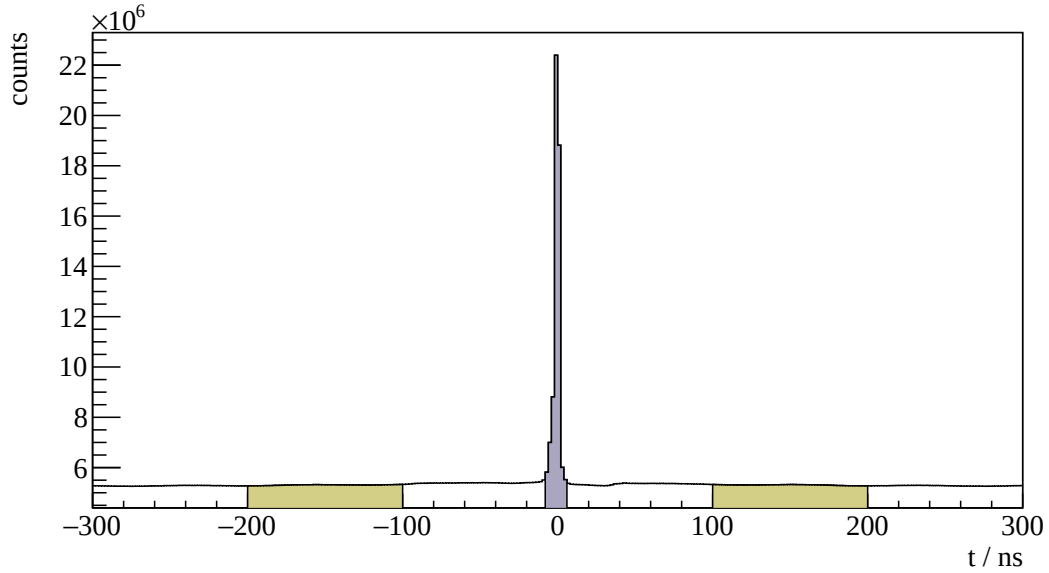

Figure 3.3: Reaction time t_r for 3PED η' production

3.3 Kinematic constraints

Up until now mainly combinatorical background was discussed. However one can derive kinematical constraints from energy and momentum conservation to exclusively select the desired reaction. The derivation is discussed first, followed by the determination of the derived cut conditions.

3.3.1 Derivation of cut conditions

After charge and time cut, additional cuts can be derived from energy and momentum conservation. Let p_{beam} and p_p be the four momenta of the initial state beam photon and proton, respectively. Then

$$p_{\text{beam}} + p_p = p_{\text{recoil}} + p_{\text{meson}} \tag{3.2}$$

holds, with p_{recoil} being the momentum of the recoiling proton and p_{meson} the meson momentum.

Coplanarity

In the initial state there is vanishing transversal momentum p_{xy} since the target protons are at rest and the beam photon impinges in z-direction. Naturally this transversal momentum has to vanish in the final state as well, such that

$$\mathcal{P}_{xy}\left[p_{\text{recoil}} + p_{\text{meson}}\right] = 0, \tag{3.3}$$

where $\mathcal{P}_{xy}$ is the projection operator to the transversal plane. Equation (3.3) is valid if and only if meson and proton lie back to back (coplanar) in the x-y plane, which is quantified by the difference of their azimuthal angles ϕ_{meson} and ϕ_{recoil} being 180° in the laboratory-frame

$$\Delta\phi := \phi^{\text{LAB}}_{\text{meson}} - \phi^{\text{LAB}}_{\text{recoil}} \stackrel{!}{=} 180^\circ. \tag{3.4}$$

Polar angle difference

If all initial and final state momenta are measured, the reaction described by equation (3.2) is *overdetermined*, such that one final state particle can be treated as a "missing particle" X with momentum p_X:

$$p_X = p_{\text{beam}} + p_p - p_{\text{meson}}. \tag{3.5}$$

One can then use

$$\Delta\theta := \theta^{\text{LAB}}_{p_X} - \theta^{\text{LAB}}_{p_{\text{recoil}}} \stackrel{!}{=} 0 \tag{3.6}$$

as a further constraint to the data.

Missing mass

The previously described angular cuts are only applicable if all final state particles have been detected. Independently of the detection of the recoil proton the mass of the missing particle $m_X^2 = p_X^2$ can be determined and compared with the proton mass of $m_p = 938.27\,\text{MeV}$ [Zyl+20]. From equation (3.5) it follows that

$$m_X = \sqrt{(E_\gamma + m_p - E_{\text{meson}})^2 - p_{x,\text{meson}}^2 - p_{y,\text{meson}}^2 - (E_\gamma - p_{z,\text{meson}})^2}. \tag{3.7}$$

Invariant mass

The measurement of the invariant mass of the two final state photons does also not require the measurement of the recoil proton. The knowledge of both four-momenta suffices, since

$$m_{\text{meson}} = \sqrt{p_{\text{meson}}^2} = \sqrt{(p_{\gamma_1} + p_{\gamma_2})^2} = \sqrt{2E_{\gamma_1}E_{\gamma_2}(1 - \cos\alpha_{\gamma_1\gamma_2})}, \tag{3.8}$$

where E_{γ_i} are the measured photon energies and $\alpha_{\gamma_1\gamma_2}$ is the angle spanned by the two photon momenta. To select only η' candidates $m_{\text{meson}} = m_{\eta'} = 957.78\,\text{MeV}$ is demanded. Remarkably, the cut on the invariant mass of the final state photons is the only one to uniquely select η' production candidates so far. All other cuts apply similarly to arbitrary meson photoproduction.

3.3.2 Determination of cut ranges

The constraints described in the previous section must not be understood as strict equalities, cf. equations (3.3),(3.6),(3.7) and (3.8). The quantities of interest will rather describe distributions around the desired value, such that confidence intervals may be extracted by fitting to said distributions. This is done iteratively:

Let C_I^χ be the cut operator that restrains the data $\mathcal{D}$ such that the (generic) cut variable

$$\chi \in \{\Delta\theta, \Delta\phi, m_X, m_{\text{meson}}\}$$

lies in the interval $\mathcal{I} \subseteq \mathbb{R}$, such that

$$C_I^\chi : \mathcal{D} \mapsto \mathcal{D}_{\chi\in\mathcal{I}}. \tag{3.9}$$

After a first inspection of the data, initial guesses for the intervals $\mathcal{I}, \mathcal{J}, \mathcal{K}, \mathcal{L}$ corresponding to the quantities $\Delta\theta, \Delta\phi, m_X, m_{\text{meson}}$ respectively are made. Having established estimates for the cut ranges,

new ones are estimated by investigating the distribution of one cut variable obtained from the data while all other cut variables are constrained to the previously determined intervals. For example

$$\Delta\theta \left(C_{\mathcal{J}}^{\Delta\phi} C_{\mathcal{K}}^{m_X} C_{\mathcal{L}}^{m_{\text{meson}}} \mathcal{D} \right) \sim \text{normal}(\mu, \sigma),$$

where $\mu \approx 0$. This is done (with some adjustments to the fit function) for each cut variable. The parameters of the gaussian are determined from a χ^2 fit and used to assign new cut ranges. Simultaneously, Monte-Carlo (MC) data of relevant final states are fitted to match the measured values bin-wise. This is done on the one hand to check consistency between measured and MC data and on the other hand used to determine contributing background reactions. First, all mesonic final states that decay into two photons are considered, i.e. $p\pi^0, p\eta, p\eta'$, since the according peaks in the invariant mass spectrum will be visible. Also, a peak at the mass of the ω (vector)-meson m_ω will be visible; this stems from photoproduction reactions $p\omega \to p\pi^0\gamma \to p3\gamma$ where one low energetic final state photon is lost, such that the reconstructed invariant mass still estimates the ω mass. Further, one should investigate the impact of neutral final states, where some of the final state photons may get lost during reconstruction, as can be observed for $p2\pi^0, p\pi^0\eta, p3\pi^0, p2\pi^0\eta$ [1] production. Lastly, possible misidentifiaction of charged particles which then mimic a $p\gamma\gamma$ final state are examined, such as $p\pi^+\pi^-$ and $n\pi^+$. Table 3.2 lists all employed MC reactions and their respective final state particles, as well as a short explanation why the particular reaction was included in the fit.

Photoproduction reaction	Final state particles	Explanation
$p\pi^0$	$p\gamma\gamma$	prominent peak in the invariant mass spectrum
$p\eta$	$p\gamma\gamma$	
$p\omega$	$p\pi^0\gamma \to p3\gamma$	
$p\eta'$	$p\gamma\gamma$	
$p2\pi^0$	$p4\gamma$	lost photons cause a ”3-particle” final state
$p\pi^0\eta$	$p4\gamma$	
$p3\pi^0$	$p6\gamma$	
$p2\pi^0\eta$	$p6\gamma$	
$p\pi^+\pi^-$		misidentification of charged particles
$n\pi^+$		

Table 3.2: Examined MC reactions that were used in sum for the fit

Since the invariant mass spectrum features rich contributions from many final states, it is difficult to describe by a (sum of) gaussian function(s), especially considering the background contributions. Thus, for the invariant mass the cut ranges are obtained from gaussian fits to the scaled MC data of the η' final state. Table 3.3 shows which fit function and cut range was used for each cut variable. In addition, it shows if the cut ranges were determined from MC or measured data. The newly obtained intervals $\mathcal{I}', \mathcal{J}', \mathcal{K}', \mathcal{L}'$ serve again as input for the previous step. This is repeated until a certain convergence is reached, which is usually the case after a two or three iterations. Since the cut ranges may vary depending on beam energy and meson direction, they are determined in bins of the beam

[1] all mesons m decaying into two photons is implied: $m \to \gamma\gamma \forall m$

cut variable	fit function	interval range	obtained from
$\Delta\theta$	Gauss	$\mathcal{I}' = [\mu - 3\sigma, \mu + 3\sigma]$	data points
$\Delta\phi$	Gauss	$\mathcal{J}' = [\mu - 3\sigma, \mu + 3\sigma]$	data points
m_X	Novosibirsk [Ike+00]	$\mathcal{K}' = [\mu - 2\sigma, \mu + 2\sigma]$	data points
m_{meson}	Gauss	$\mathcal{L}' = [\mu - 2\sigma, \mu + 2\sigma]$	MC data

Table 3.3: Fit functions and cut ranges for each variable

energy and the CMS polar angle of the meson

$$(E_\gamma, \cos\theta_{\eta'}^{\text{CMS}})^2.$$

Respecting the η' final state statistics, a binning of $\Delta E_\gamma = 100\,\text{MeV}$ and $\Delta\cos\theta = 1/3$ was chosen, spanning the energy range of 1 500 to 1 800 MeV. The theoretically accessible lower limit in the beam energy is provided by the production threshold of η' mesons at 1 447 MeV [Zyl+20]. Yet, the binning has to comply with the upper beam energy limit which is bounded from above [3] by the position of the coherent edge of the beamtime. It is given by 1 700 MeV and 1 800 MeV for the July/August and September/October beam times, respectively. If one were to include the production threshold into the analyzed range using the same binning, more background than η' events are collected from 1 400 to 1 500 MeV, hence the chosen binning starts at 1 500 MeV.

Coplanarity

Figure 3.4 shows the coplanarity spectra for the energy bin $1\,500\,\text{MeV} \leq E_\gamma < 1\,600\,\text{MeV}$ and all angular bins. The data points are visualized by the open circles with error bars, while the black solid histogram is a fit of $\eta' \to \gamma\gamma$ MC. As expected, a clear peak is visible at $\Delta\phi = 180^\circ$, which shows only slight dependence on beam energy and meson direction. A 3σ interval obtained from a gaussian fit is indicated by the dashed red lines. Note that only MC spectra of the η' final state were fitted to the data since the coplanarity gives little reference points for other final states that may contribute.

Polar angle difference

Since the meson direction correlates with the detector(s) the final state photons hit, the polar angle difference depicts a clear directional dependence as can be seen in figure 3.5 for the energy bin $1\,500\,\text{MeV} \leq E_\gamma < 1\,600\,\text{MeV}$ and all angular bins. In the CMS frame, meson and proton are emitted back to back. Thus, if the meson is emitted in backward direction ($\cos\theta \sim -1$), the proton will be detected either in the forward or MiniTAPS detector, which have a better angular resolution than the Crystal Barrel calorimeter, leading to narrower distributions of $\Delta\theta$. The determined cut ranges are 3σ intervals obtained from a gaussian fit to the data and are indicated by the red dashed lines. As before, no other than η' MC are fitted to the spectra.

[2] If not otherwise specified, from now on $\cos\theta = \cos\theta_{\eta'}^{\text{CMS}}$

[3] Significantly beyond the coherent edge, the systematic error for the beam polarization degree gets too large (> 10%)

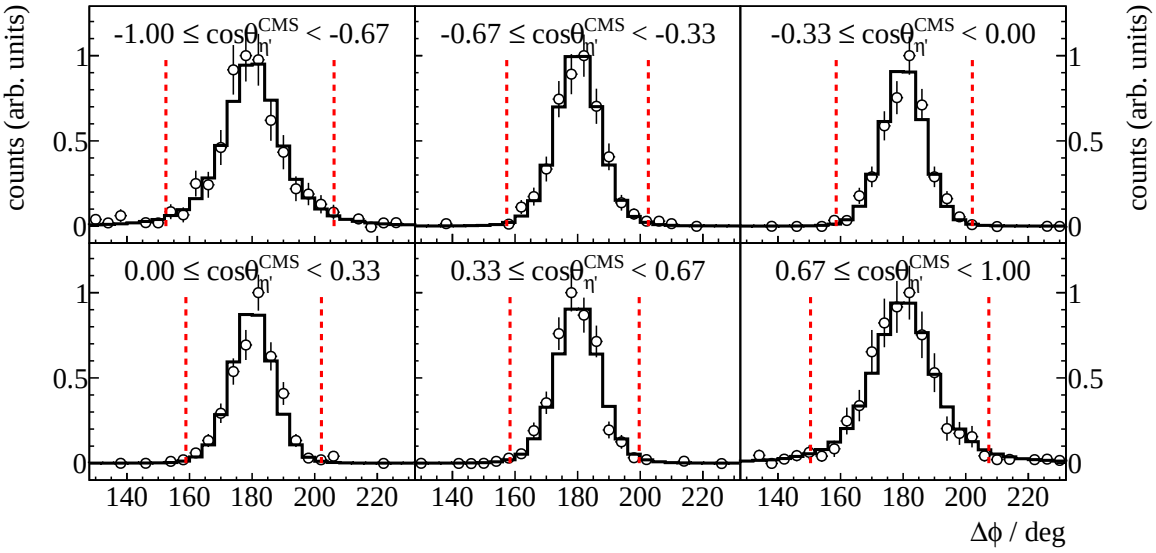

Figure 3.4: Coplanarity of the $p\eta'$ final state with all other cuts applied for the energy bin 1 500 MeV $\leq E_\gamma <$ 1 600 MeV. The vertical dashed lines show the cut ranges obtained from a gaussian fit to the data (open circles). The solid black histograms represent fitted MC data of $\eta' \to \gamma\gamma$

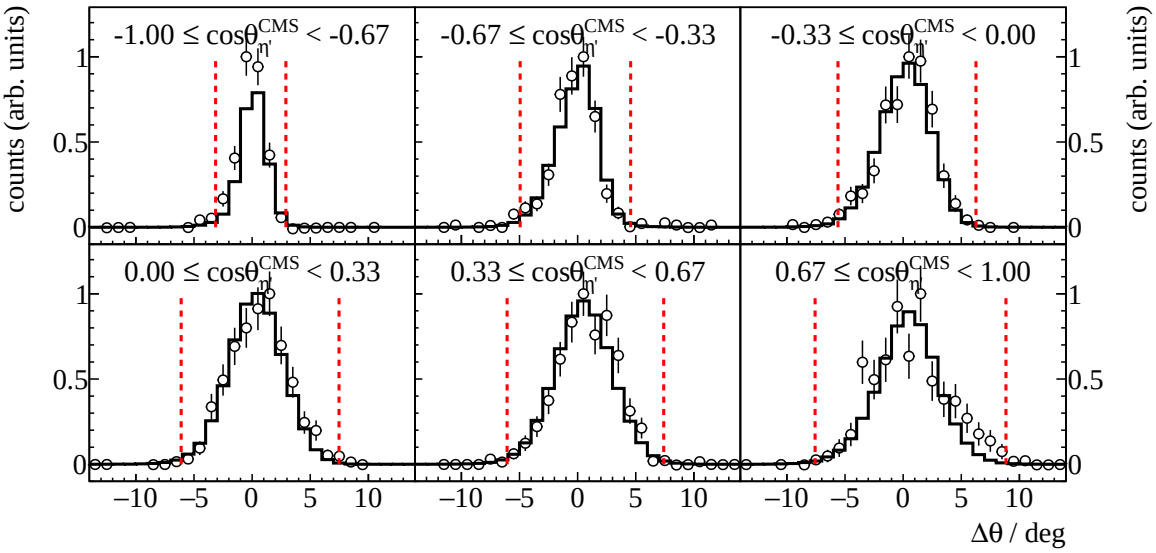

Figure 3.5: Polar angle difference of the $p\eta'$ final state with all other cuts applied for the energy bin 1 500 MeV $\leq E_\gamma <$ 1 600 MeV. The vertical dashed lines show the cut ranges obtained from a gaussian fit to the data (open circles). The solid black histograms represent fitted MC data of $\eta' \to \gamma\gamma$

Missing mass

The missing mass spectra allow a first investigation of possible background reactions that pass event selection. For all angular bins of the first energy bin the missing mass is shown in figure 3.6; again, the open circles are the data points with corresponding statistical error bars. The solid colored histograms are fitted MC spectra of different possible background contributions while the black histogram is the signal contribution of $\eta' \to \gamma\gamma$ photoproduction. The turquoise histogram is the sum of all MC histograms. Generally, most of the data can be described by the η' MC alone, but especially towards higher masses (and higher beam energies) background contributions extend the missing mass peak as flat background. These are reactions where the reconstructed meson mass $m^2_{\text{meson}} = E^2_{\text{meson}} - \vec{p}^2_{\text{meson}}$ is smaller than the η' mass, resulting in larger values for the missing mass. Judging from the fit to the missing mass, $2\pi^0$ and/or $\pi^0\eta$ photoproduction may describe the background as both show similar shapes. All other previously mentioned reactions (table 3.2) do not contribute significantly. Better conclusions can be drawn from the invariant mass spectra as is discussed in the following section 3.4. The cut ranges for the missing mass are obtained from a Novosibirsk [Ike+00] fit to the data since the missing mass distribution is slightly asymmetric. However, since the tail parameter is small, still a symmetric cut of $\pm 2\sigma$ was chosen. It was chosen narrower than the angular cuts to collect less background reactions.

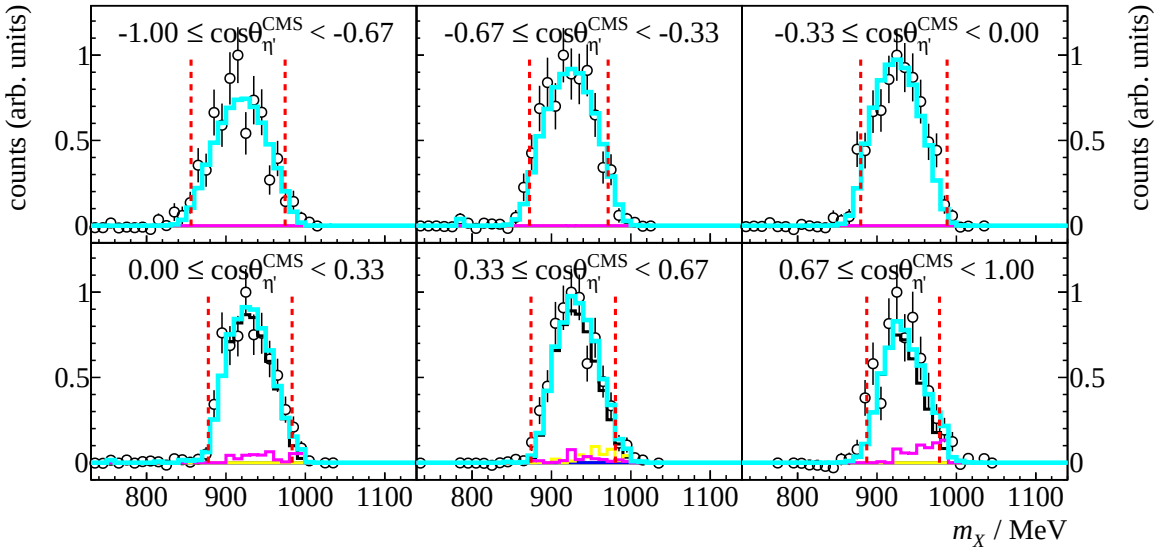

Figure 3.6: Missing mass of the $p\eta'$ final state with all other cuts applied for the energy bin 1 500 MeV $\leq E_\gamma <$ 1 600 MeV. The vertical dashed lines show the cut ranges obtained from a fit to data (open circles) employing a Novosibirsk function. The solid colored histograms represent fitted MC data from relevant photoproduction reactions: in black η', in green π^0, in red η, in blue ω, in yellow $2\pi^0$, magenta $\pi^0\eta$. The turquoise histogram is the sum of all MC histograms.

Invariant mass

Investigating the invariant mass spectrum of the final state photons allows to illustrate the impact of the event selection so far. As has been mentioned all cuts considered up to this point apply to arbitrary meson photoproduction. This means that the invariant mass spectrum will depict peaks belonging to mesons produced in the considered beam energy range. This is shown in figure 3.7 giving an overview over all energy and angular bins. All other cuts have been applied. The open circles represent data points and the different colored histograms MC data from relevant competing final states while the black histogram shows the signal contribution of η' MC. The turquoise histogram is the sum of all MC contributions and describes the data very well. It has again been found that no other than the shown final states contribute significantly or improve the description of data by MC spectra. As expected one can observe peaks belonging to π^0, η, ω and η' photoproduction. A flat background underneath the complete spectrum is realized by $2\pi^0$ and $\pi^0\eta$ final state photons that have been wrongfully combined to two photons. Remarkably, the π^0, η and ω invariant mass distributions also depict long tails towards lower and higher masses, although they contribute only marginally to the sum of all MC spectra (note the logarithmic y-Scale). They can be explained by the fact that one low energetic photon is lost during reconstruction while the (high energetic) proton wrongfully creates two tracks of which one is then combined with the other photon as meson candidate [Afz19]. To finally select only η'

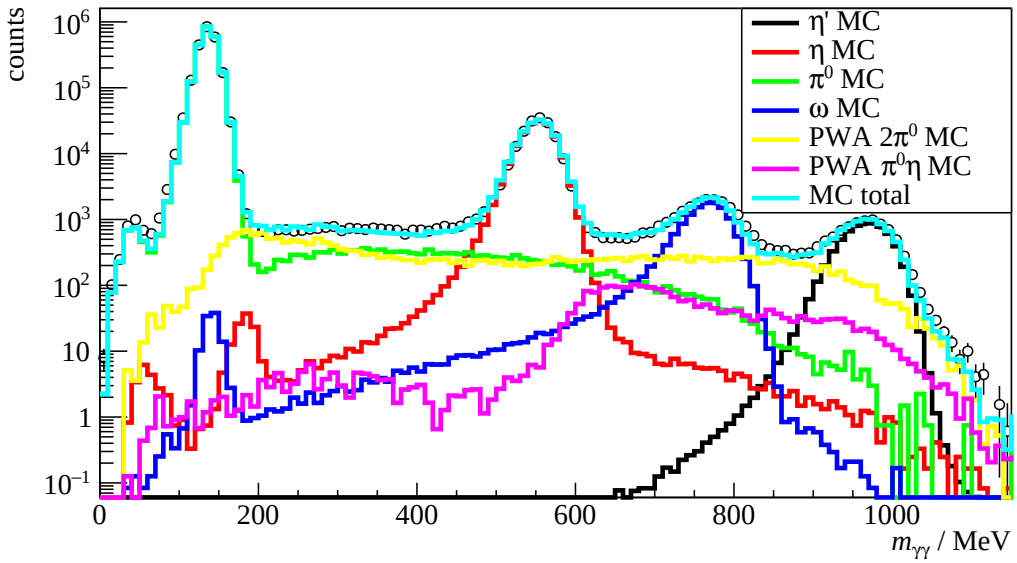

Figure 3.7: Invariant mass of the $p\eta'$ final state with all other cuts applied for all energy and angular bins. The open circles represent the measured data, the solid colored histograms fitted MC data from relevant photoproduction reactions: in black η', in green π^0, in red η, in blue ω, in yellow $2\pi^0$ and in magenta $\pi^0\eta$. The turquoise histogram is the sum of all MC histograms.

photoproduction event candidates the invariant mass cut is determined again in bins of beam energy and meson polar angle. This is shown in figure 3.8 for the first energy bin with all angular bins. Here, the same color coding as before applies, but the range of the invariant mass has been reduced to only cover the η' peak for visibility's sake. Additionally the cut ranges, representing a 2σ interval obtained

from a gaussian fit to the η' MC, are shown as dashed, red lines. Considering the statistics the MC spectra still describe the data well. It is found again that the significant background contributions in the invariant mass range of interest are given by $2\pi^0$ and $\pi^0\eta$ photoproduction.

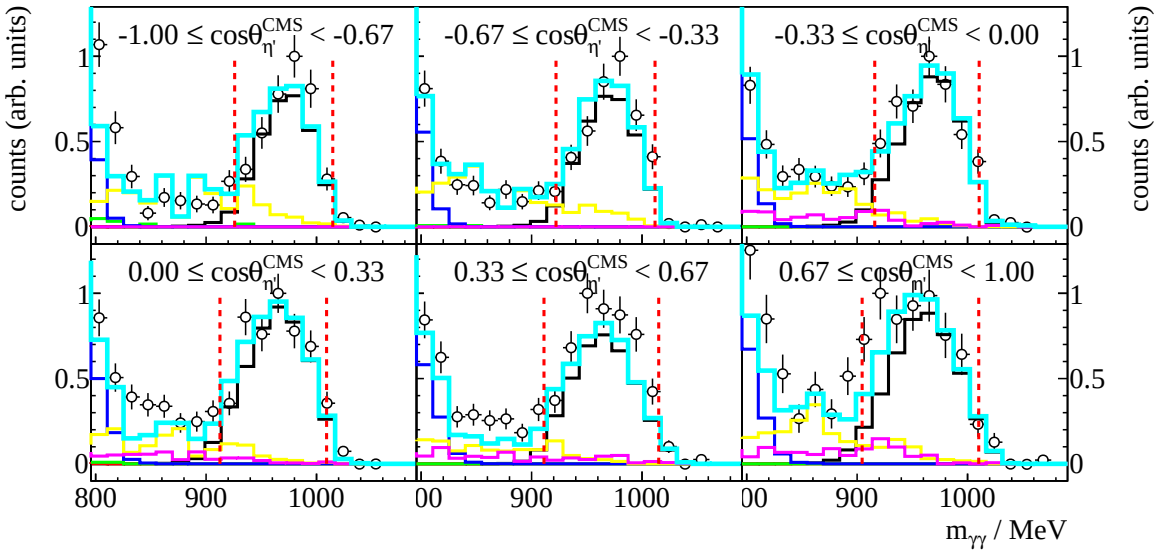

Figure 3.8: Invariant mass of the $p\eta'$ final state with all other cuts applied for the energy bin 1 500 MeV ≤ E_γ < 1 600 MeV. The vertical dashed lines show the cut ranges obtained from a gaussian fit to the η' MC data (solid black histogram). The open circles represent the measured data, the solid colored histograms fitted MC data from relevant photoproduction reactions: in black η', in green π^0, in red η, in blue ω, in yellow $2\pi^0$ and in magenta $\pi^0\eta$. The turquoise histogram is the sum of all MC histograms.

3.3.3 Quality of event selection

In order to investigate the impact of applied cuts the detector and analysis acceptance $A(E_\gamma, \cos\theta)$ can be investigated. It is defined as the ratio of reconstructed events $N^{\text{rec}}(E_\gamma, \cos\theta)$ to generated events $N^{\text{gen}}(E_\gamma, \cos\theta)$

$$A := \frac{N^{\text{rec}}(E_\gamma, \cos\theta)}{N^{\text{gen}}(E_\gamma, \cos\theta)} \tag{3.10}$$

and is shown in figure 3.9. Acceptance holes are visible in very forward and in backward direction which can be contributed to events where the proton escapes the calorimeters or is absorbed in insensitive material. Also, events close to threshold are unlikely to be reconstructed which can also be explained by low energy protons. A maximum acceptance of $\tilde{A} \approx 0.61$ is reached which can be understood considering the cuts that have been made; each 3σ cuts retains 99% of events and each 2σ cut 95%. Assuming detection efficiencies of 90% for the two uncharged photons and 85% for the charged proton ([Afz19; Har17]) it is evident that $0.99^2 \cdot 0.95^2 \cdot 0.9^2 \cdot 0.85 \approx 0.61$. In total, $8 \cdot 10^3$ η' events were extracted which nonetheless still contain background contaminations. In order to take this into account in the later analysis the fraction of background is determined for each bin in beam

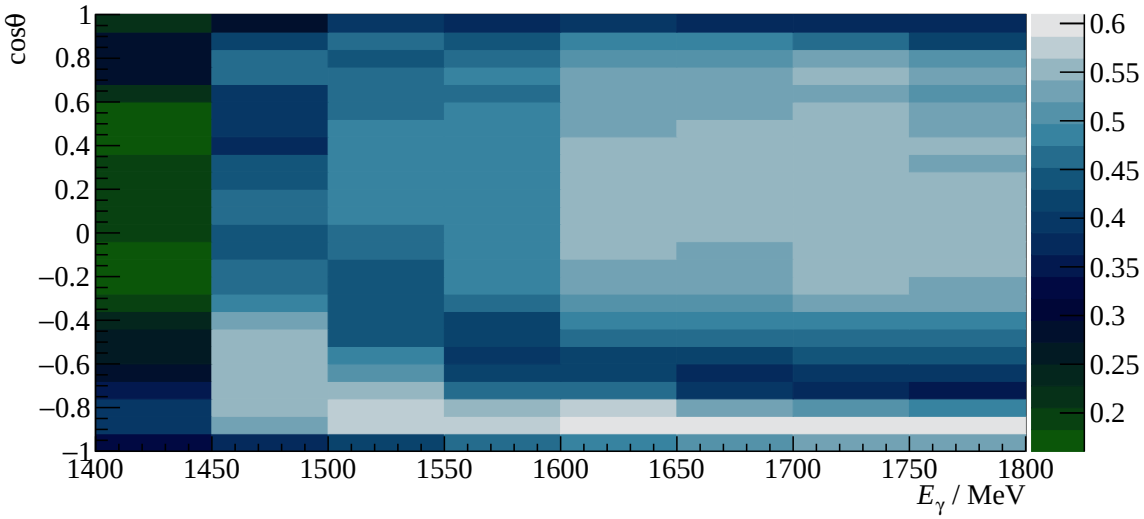

Figure 3.9: Acceptance for the reaction $\gamma p \to p\eta'$ after all cuts that have been discussed so far for 2.5PED and 3PED events

energy and meson polar angle. It is estimated as the fraction of background MC events to total MC events and shown in figure 3.10. For most bins around 15% of all events are misidentified as η' events. Especially at very forward $\cos\theta \to 1$ and backward $\cos\theta \to -1$ angles the background contributions are significantly higher, reaching up to 45%.

3.4 Investigation of background and additional cuts

So far the background reactions in the η' cut ranges have been discussed only phenomenologically as they describe the measured invariant mass spectra best. In the following the plausibility and causality of these background contributions shall be discussed. Furthermore it is investigated if the found background contributions may be reduced or eliminated by additional cut conditions.

3.4.1 Inspecting plausibility of background reactions

To evaluate the likelihood that the background contributions are made up of $2\pi^0$ or $\pi^0\eta$ production events the respective production cross sections in the inspected beam energy region and branching ratios (BR) to purely photonic final states are examined, see table 3.4. Also displayed is the maximum acceptance $\tilde{A}$ which is additionally shown in figure 3.11. Both possible background reactions exceed η' photoproduction in cross section and also in relative frequency of purely photonic final states. At the same time the acceptance is almost vanishing, proving that the kinematic cuts are generally very effective.

Since the total number of events is proportional to the cross section σ, branching ratio BR and

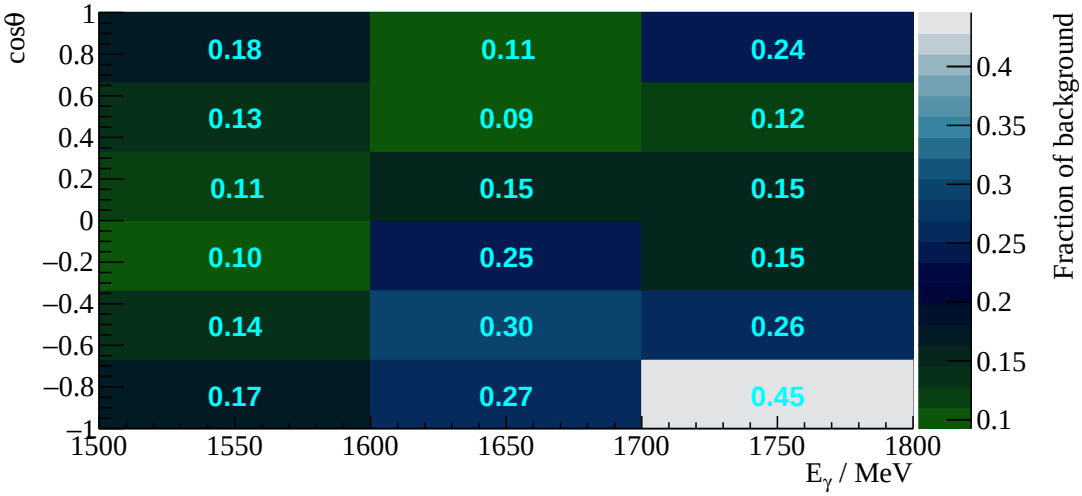

Figure 3.10: Fraction of background events in the analyzed beam energy and angular bins.

reaction	σ / µb	BR to $n\gamma$	$\tilde{A}$
$\gamma p \to p\eta'$	≈ 1 [Cre+09]	0.02	0.61
$\gamma p \to p2\pi^0$	$\lesssim 5$ [Die+20]	$0.98^2 = 0.96$	$7 \cdot 10^{-4}$
$\gamma p \to p\pi^0\eta$	≈ 3 [Käs+18]	$0.98 \cdot 0.38 = 0.37$	$2 \cdot 10^{-4}$

Table 3.4: Total cross sections σ in the energy range 1 500 to 1 800 MeV and branching ratios (BR) to $n\gamma$ final states for signal and possible background contributions

acceptance $\tilde{A}$, the ratio of reconstructed background to signal events is then given by

$$R = \frac{\sigma \cdot \mathrm{BR} \cdot \tilde{A}}{\sigma_{\eta'} \cdot \mathrm{BR}_{\eta' \to \gamma\gamma} \cdot \tilde{A}_{\eta'}} = \frac{\sigma \cdot \mathrm{BR} \cdot \tilde{A}}{1\,\mu\mathrm{b} \cdot 0.02 \cdot 0.61}.$$

One finds $R \lesssim 0.3$ and $R \lesssim 0.05$ for $2\pi^0$ and $\pi^0\eta$ photoproduction, respectively. Although less than 0.1% of two meson production reactions are misidentified as η' events they make up a significant portion of background in η' data, as considering the according branching ratios and cross sections showed. Furthermore, the previous empirical assumption to only include $2\pi^0$ and $\pi^0\eta$ MC in the fit to describe the data is now justified since the found background percentages agree well with the now motivated upper boundaries.

3.4.2 Misidentification of background reactions

3.4.3 Examination of additional cuts

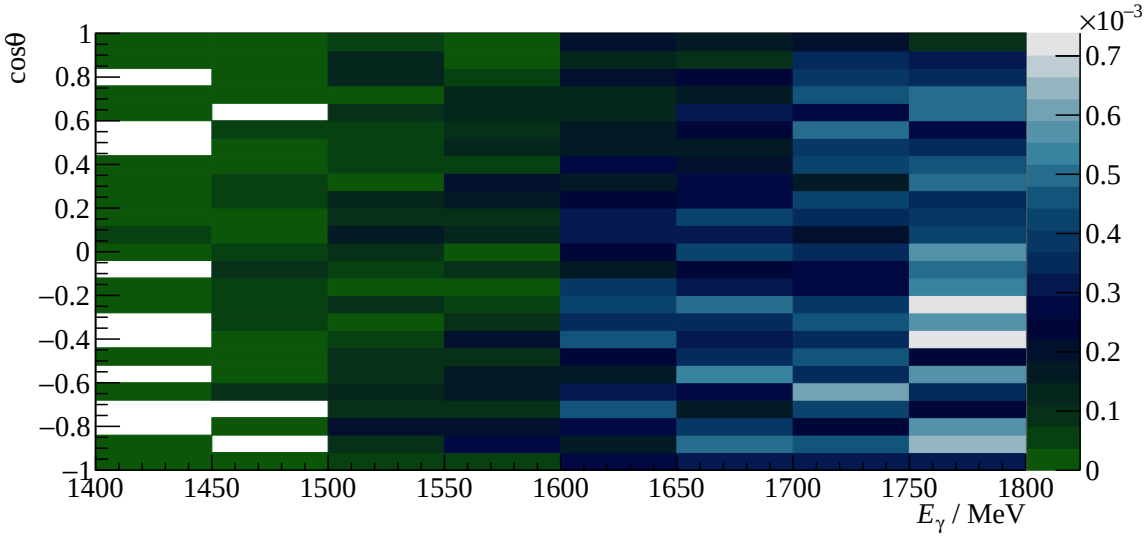

(a) $\gamma p \to p2\pi^0$

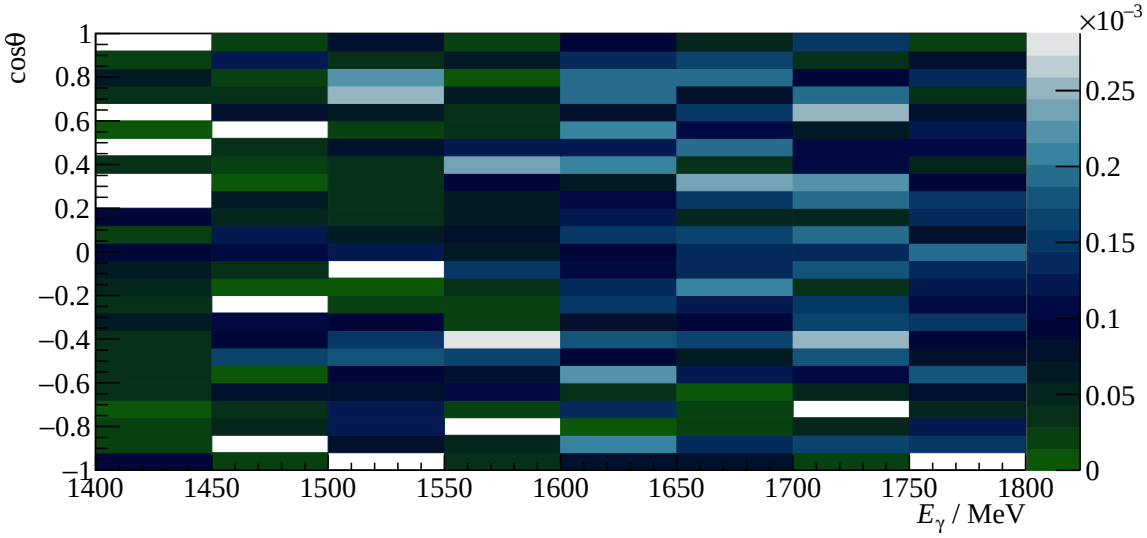

(b) $\gamma p \to p\pi^0\eta$

Figure 3.11: Acceptance for possible background contributions

Bibliography

[Afz22] F. Afzal, *Private communication*, 2022 (cit. on p. 11).

[Zyl+20] P. Zyla et al., *Review of Particle Physics*, PTEP **2020** (2020) 083C01 (cit. on pp. 11, 15, 17).

[Afz19] F. N. Afzal, *Measurement of the beam and helicity asymmetries in the reactions $\gamma p \to p\pi^0$ and $\gamma p \to p\eta$*, PhD thesis: Rheinische Friedrich-Wilhelms-Universität Bonn, 2019, URL: https://hdl.handle.net/20.500.11811/8064 (cit. on pp. 11, 20, 21).

[Ike+00] H. Ikeda et al., *A detailed test of the CsI(Tl) calorimeter for BELLE with photon beams of energy between 20-MeV and 5.4-GeV*, Nucl. Instrum. Meth. A **441** (2000) 401 (cit. on pp. 17, 19).

[Har17] J. Hartmann, *Measurement of Double Polarization Observables in the Reactions $\gamma p \to p\pi^0$ and $\gamma p \to p\eta$ with the Crystal Barrel/TAPS Experiment at ELSA*, Rheinische Friedrich-Wilhelms-Universität Bonn, 2017, URL: https://hdl.handle.net/20.500.11811/7258 (cit. on p. 21).

[Cre+09] V. Crede et al., *Photoproduction of eta and eta-prime mesons off protons*, Phys. Rev. C **80** (2009) 055202, arXiv: 0909.1248 [nucl-ex] (cit. on p. 23).

[Die+20] M. Dieterle et al., *Helicity-Dependent Cross Sections for the Photoproduction of π^0 Pairs from Nucleons*, Physical Review Letters **125** (2020), URL: https://doi.org/10.1103%2Fphysrevlett.125.062001 (cit. on p. 23).

[Käs+18] A. Käser et al., *First measurement of helicity-dependent cross sections in $\pi 0\eta$ photoproduction from quasi-free nucleons*, Physics Letters B **786** (2018) 305, URL: https://doi.org/10.1016%2Fj.physletb.2018.10.006 (cit. on p. 23).

List of Figures

List of Tables